NJC

ROYAL SOCIETY OF CHEMISTRY

PAPER

View Article Online
View Journal | View Issue

Cite this: *New J. Chem.*, 2025, **49**, 5248

Systematic analysis of the material basis and potential mechanism of Banxia Houpo Decoction against chronic pharyngitis based on chemical and metabolite profile characterization combined with network pharmacology†

Yanru Liu,[a] Jiayi Zheng,[a] Lu Shen,[a] Gongjun Yang*[ab] and Fang Feng *[ab]

Banxia Houpo Decoction (BXHPD), a Traditional Chinese medicine (TCM) prescription, is commonly used to treat chronic pharyngitis. However, the material basis and potential mechanisms of BXHPD against chronic pharyngitis have not been clarified. UPLC-Q-Exactive Orbitrap-MS, a quadrupole exactive orbitrap tandem mass spectrometer combined with ultra-high performance liquid chromatography, was utilized in this work to investigate the chemical components of BXHPD and their prototypes or metabolites *in vivo*. Then, the protein–protein interaction and the "absorbed component–target–pathway-disease" networks were established to elucidate its potential mechanism. Employing this thorough investigation, 121 chemical compounds were identified in the BXHPD. Meanwhile, 50 exogenous components (23 prototype components and 27 metabolic components) were examined in rat plasma. Furthermore, network pharmacology and molecular docking revealed that magnoflorine, apigenin, honokiol, randainal, and magnolignan A with related targets AKT1, MAPK1, MAPK3, EGFR, PIK3R1, RELA, PIK3CA, NFKB1, and CCND1 were considered as the effective components and core targets. Besides, the results also indicated that PI3K-Akt, TNF, and MAPK signaling pathways might contribute significantly to the therapeutic effects of BXHPD on chronic pharyngitis. The outcomes of molecular docking and molecular dynamics simulations show that the key targets have strong binding capacities with effective components. BXHPD may have anti-inflammatory and antibacterial properties as part of its several modes of action against chronic pharyngitis. A broader range of medicinal applications is made possible by our research, which offers a comprehensive method for examining the molecular basis and underlying mechanisms of BXHPD against chronic pharyngitis.

Received 23rd November 2024,
Accepted 1st March 2025

DOI: 10.1039/d4nj05045b

rsc.li/njc

Introduction

An ongoing inflammation of the lymphoid tissue, pharyngeal mucosa, and submucosa is known as chronic pharyngitis.[1] A dry throat, itchy, painful throat, pharyngeal foreign body sensation, dry cough, and decreased mucus production are the clinical indications of chronic pharyngitis.[2] Common causes of chronic pharyngitis, an inflammation of the pharyngeal mucosa, include viruses, germs, alcohol misuse, voice abuse, and smoking.[3] According to epidemiological data, chronic pharyngitis affects at least 20% of individuals worldwide,[4] and the World Health Organization (WHO) has classified chronic pharyngitis as a sub-health condition.[5] Patients' quality of life is significantly impacted by the characteristics of chronic pharyngitis, which include high prevalence, a protracted course, a complex etiology, stubborn symptoms, and difficult therapy.[6] Aerosol inhalation and antibiotics are the two main therapies used for chronic pharyngitis. Addiction to antibiotics can result in medication resistance, and misuse can cause an imbalance in the flora in the throat, which can cause a relapse of the illness and much more damage.[7] Even though atomization can have some curative effects, patients often lose faith in atomization treatment because it is difficult to heal and frequently occurs repeatedly.[8] Finding alternative and complementary therapy is therefore essential for treating chronic pharyngitis.

[a] *Department of Pharmaceutical Analysis, China Pharmaceutical University, Longmian Avenue No. 639, Nanjing 210009, China. E-mail: lyr2674990839@163.com, 1240685547@qq.com, 1131472230@qq.com, gjyang@cpu.edu.cn, fengfang1@hotmail.com*

[b] *Key Laboratory of Drug Quality Control and Pharmacovigilance (China Pharmaceutical University), Ministry of Education, China Pharmaceutical University, Nanjing 210009, China*

† Electronic supplementary information (ESI) available. See DOI: https://doi.org/10.1039/d4nj05045b

The use of Traditional Chinese medicines (TCM) has gained popularity recently due to the notable advantages of reducing clinical symptoms, enhancing the effectiveness of therapy, providing consistent therapeutic efficacy, and being safe. A well-known TCM prescription that is frequently utilized in clinical practice is Banxia Houpo Decoction (BXHPD). BXHPD comes from ''Jin Gui Yao Lue'', which was initially documented in the Han Dynasty (202 BC-220 AD). Five herbal medications are included in BXHPD: dried tuber of *Pinellia ternata* (Thunb.) Breit. (Banxia in China, BX); fresh rhizomes of *Zingiber officinale* Rose. (Shengjiang in China, SJ); dried cortex of *Magnolia officinalis* Rehd. et Wils. (Houpo in China, HP); dried fungus sclerotium of *Poria cocos* (Schw.) Wolf. (Fuling in China, FL); and dried leaves of *Perilla frutescens* (L.) Britt (Zisuye in China, ZSY). In clinic, BXHPD is typically used for treating psychiatric disorders and digestive system diseases such as depression,[9] peptic ulcer,[10] functional dyspepsia,[11] and bowel ileus,[12] especially for treating chronic pharyngitis.[13] However, the unidentified active ingredients and processes for treating chronic pharyngitis limit the development and use of BXHPD.

Since the components of TCM prescriptions, especially the prototypes and their metabolites *in vivo*, may play a role in mediating therapeutic efficacy. Gaining a thorough grasp of the chemical constituents and metabolic profiles of BXHPD is essential for elucidating underlying mechanisms and improving clinical applications. Research on BXHPD mainly focuses on clinical application and pharmacological effects. At present, there is little research on the chemical composition of the prescription.[14,15] Regarding the metabolic profile and pathway connected to the BXHPD formula, no research has been done. The method for thoroughly comprehending the connections between medications, compounds, targets, pathways, and illnesses is known as network pharmacology.[16] It has the potential to create drug-target-disease networks, identify mechanisms of action, forecast active ingredients, key targets, and important pathways.[17]

The present investigation utilized an integrated methodology that involved UPLC-Q-Exactive Orbitrap-MS in conjunction with network pharmacology. This made it possible to identify the chemical and metabolic properties of BXHPD in rats and elucidate the components and mechanisms of action that work best for treating chronic pharyngitis. The four main aspects of this study were (Fig. 1): (1) systemic characterization of the chemical composition of BXHPD extracts; (2) characterizing the prototype components and metabolic profiles of BXHPD in rat plasma; (3) identifying putative active components and the

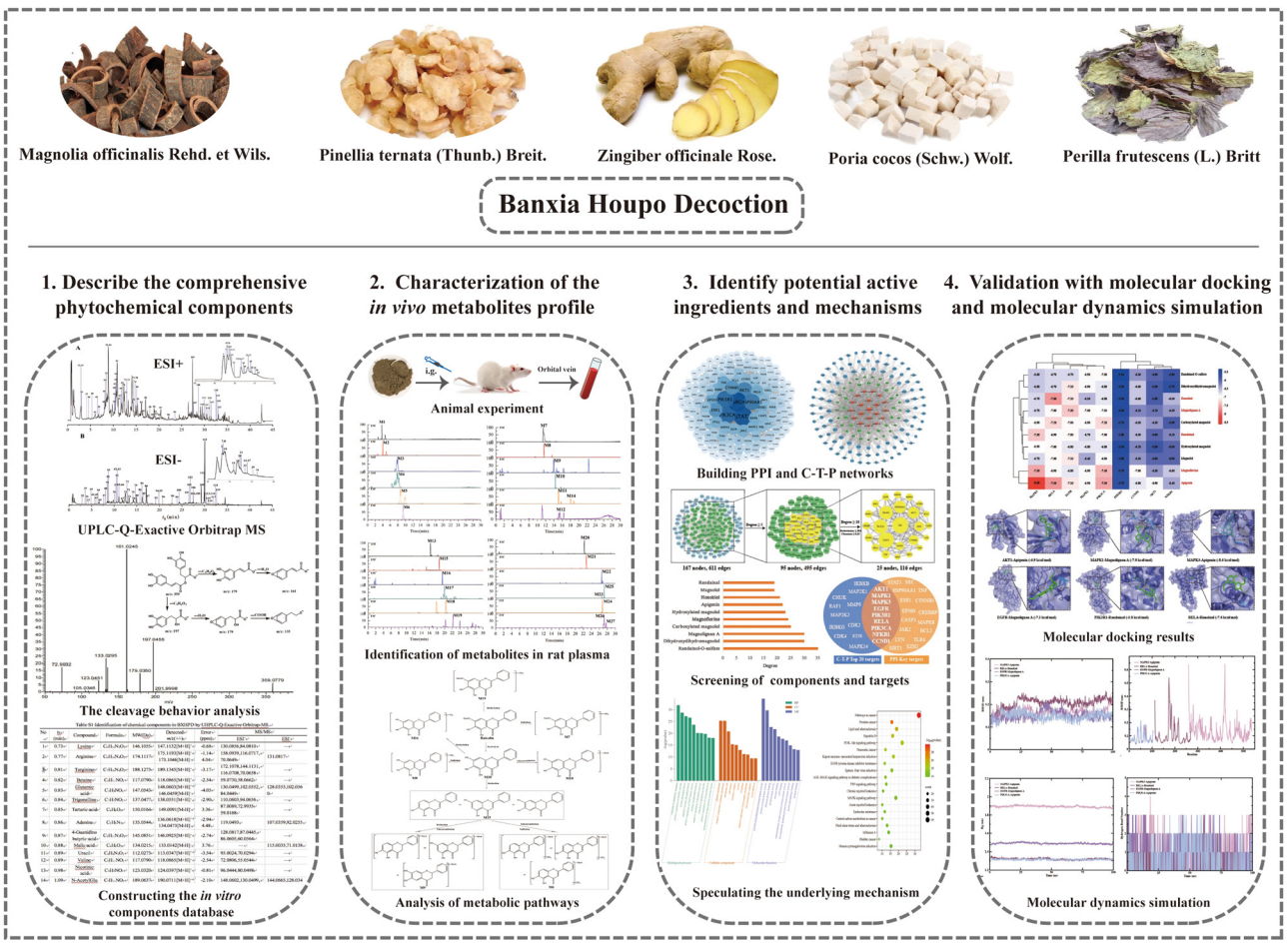

Fig. 1 The workflow of this study.

action mechanisms through network pharmacology; (4) the binding ability validation of relevant targets and components through molecular dynamics simulation and molecular docking. The investigation has some guiding implications for the clinical application of BXHPD and the investigation of its pharmacodynamic mechanisms in the treatment of chronic pharyngitis.

Materials and methods

Chemicals and herbs

Acetonitrile and methanol (LC-MS grade) were obtained from Merck (Darmstadt, Germany), and formic acid (HPLC grade) was supplied by Sigma-Aldrich Co. (St Louis, USA). The Wahaha Company supplied ultrapure water (Hangzhou, China) Every additional reagent that was utilized was analytical grade. Eight reference compounds including 6-gingerol, magnolol, adenosine, succinic acid, ferulic acid, apigenin, honokiol, and pachymic acid (purity $\geq$98%) were all supplied by Chengdu Must Bio-technology Co., Ltd (Sichuan, China).

Banxia (dried tuber of *Pinellia ternata* (Thunb.) Breit, BX, collection in Shandong, no. 190901), Houpo (dried cortex of *Magnolia officinalis* Rehd. et Wils., HP, collection in Hebei, no. 294200502), Fuling (dried fungus sclerotium of *Poria cocos* (Schw.) Wolf., FL, collection in Hebei, no. 201224001), Shengjiang (fresh rhizomes of *Zingiber officinale* Rosc., SJ, collection in Jiangsu, no. 220302785), and Zisuye (dried leaves of *Perilla frutescens* (L.) Britt., ZSY, collection in Hebei, no. 112201201) authenticated by Professor Minjian Qin (Department of Chinese Materia Medica, China Pharmaceutical University) were purchased from Nanjing Tongrentang Pharmaceutical Co., Ltd (Nanjing, China).

Preparation of reference standards and BXHPD extracted sample

Before being soaked in water (1 : 10, w/v) for 0.5 h, the raw plant materials were crushed, and combined in various amounts (BX: 15 g; HP: 9 g; FL: 12 g; SJ: 15 g; ZSY: 6 g), and then boiled for 1.0 h. After filtering the extractive, the residue was once again boiled (1 : 8, w/v). A six-layer gauze filter was used to filter the combined extraction solution. The mixed filtrates were then distilled at 45 °C under reduced pressure by a rotating evaporator (RE-52CS, Shanghai Yarong Biochemical Instrument Factory, Shanghai, China). The residue was freeze-dried through a freeze-drying machine (FD-1-SD, Beijing Boyikang Lab Instrument Co., Ltd, Beijing, China). Prior to usage, the lyophilized BXHPD powder was frozen at −20 °C. To prepare the dosage samples for medication administration, the appropriate amount of the lyophilized BXHPD powder was suspended in water.

For the determination of the chemical profiling, the lyophilized BXHPD powder was extracted with 70% methanol. Then, the extraction solution was stored at 4 °C for 12 h. A 0.22 μm membrane filter was used to filter the supernatant solution in preparation for additional LC-MS analysis. Individual stock solutions of eight reference standards were respectively prepared with methanol at 1.0 mg mL^{-1}. The solutions of eight standards were prepared with methanol at 0.1 mg mL^{-1} for LC-MS analysis.

Animals and drug administration

Ten male Sprague Dawley (SD) rats (200–220 g) were supplied by Sibeifu (Beijing) Biotechnology Co., Ltd (license number: SCXK (Beijing) 2019-0010, Beijing, China). The rats were placed in conventional conditions (23 ± 2 °C, humidity of 50 ± 5%, and 12 h light/dark cycle) with standard water and food. The Ethics Committee of China Pharmaceutical University (Nanjing, China) approved all studies, that adhered to the Guidelines for the Care and Use of Laboratory Animals (US National Research Council, 1996) (permission no. SYXK⟨SU⟩2021-0011). Ten rats were segmented into two groups (n = 5): the control group and the BXHPD group. Rats in the BXHPD group were given BXHPD (15.39 g kg^{-1} day^{-1}, equivalent to three times the therapeutic dosage of BXHPD crude drug) for three days in a row. The control group rats were administered the relevant amount of water orally for three days.

Plasma sample collection and pretreatment

Before the experiments, the rats were fasted for 12 h. After the last dosage at 0.25, 0.5, 1.0, and 2.0 h, orbital venous blood of rats was taken for the BXHPD group. Following a 10-minute centrifugation at 4000 rpm and 4 °C, equal parts of plasma samples from various time points were combined. 200 μL of mixed plasma samples were pretreated with 0.6 mL of acetonitrile. After a 3-minute vortex, the samples were centrifuged for 15 min at 12 000 rpm. Subsequently, the supernatants were collected and allowed to evaporate at 40 °C through nitrogen. After being reconstituted in 150 μL of 50% methanol–water solution, the residue was centrifuged for 15 min at 12 000 rpm. Lastly, a 0.22 μm filter membrane was used to filter the supernatant in preparation for LC-MS analysis.

UPLC-Q-Exactive Orbitrap-MS analysis

Thermo Vanquish Flex UPLC chromatographic system (Thermo Scientific, San Jose, USA) with an XBridge BEH C18 column (2.1 mm × 100 mm, 2.5 μm, Waters, USA) was used to accomplish chromatographic separation at 40 °C. Methanol (B) and 0.1% formic acid aqueous solution (A) made up the mobile phase and the program as follows: 0–1.5 min, 2% B; 1.5–23 min, 2–30% B; 23–34 min, 30–98% B; 34–41 min, 98% B; 41–41.1 min, 98–2% B; 41.1–45 min, 2% B. The injection amount used for analysis was 5 μL with a flow rate of 0.3 mL min^{-1}.

Thermo Q Exactive Plus Orbitrap Mass Spectrometer (Thermo-Fisher Scientific, Waltham, MA, USA) fitted with a heated electrospray ionization (HESI) was used to perform MS condition analysis. With a mass range of m/z 100–1200 Da, the MS acquisition mode was Full MS/dd-MS^2 in positive and negative ion modes. The remaining parameters were as follows: spray voltage of 3.5/2.8 kV (ESI^+/ESI^-); sheath gas flow rate of 45 arb; capillary temperature of 350 °C; aux gas flow rate of 10 arb.

There were three different collision energies set: 20, 40, and 60 eV.

Data analysis strategy of chemical and metabolite profiling of BXHPD

Xcalibur 4.2 (Thermo Fisher Scientific, Waltham, MA, USA) was used to process the UPLC-Q-Exactive Orbitrap-MS data for reference standards, individual herbal components, BXHPD extracts, and plasma samples. To thoroughly comprehend the chemical compositions and metabolite properties of BXHPD, use the following data analysis technique. First, using information from relevant literature about five herbs, PubChem (**https://pubchem.ncbi.nlm.nih.gov/**), ChemSpider (**https://www.chemspider.com/**), MassBank (**https://www.massbank.jp/**), and ChemBank (**https://chembank.med.harvard.edu/**) databases created an internal chemical components mass database. The *in vitro* composition of BXHPD was ascertained by comparing the structural data in the self-built database with the information from MS/MS. Furthermore, using chemical compositions determined *in vitro*, the prototype compounds were found in plasma samples. Lastly, the prototype metabolic route and fragment ions helped to clarify the metabolic properties of BXHPD.

Network pharmacology analysis

The SMILES representations of the prototypes and metabolic components were imported into the SwissTargetPrediction database (**https://www.swisstargetprediction.ch/**) with the screening criterion of "Probability" >0 in order to predict targets related to components.[18] Next, in order to predict target genes linked to chronic pharyngitis, the term "chronic pharyngitis" was entered into the databases of OMIM (**https://omim.org/**), DrugBank (**https://www.drugbank.ca**), Disgenet (**https://www.disgenet.org/**), and GeneCards (**https://www.genecards.org/**). The overlapping targets between the components-related targets and the chronic pharyngitis-related targets were obtained by the Venny 2.1 platform (**https://bioinfogp.cnb.csic.es/tools/venny/**). The acquirement of the protein–protein interaction (PPI) data was from the String database (**https://cn.string-db.org/**). Next, Cytoscape 3.9.1 software was utilized to obtain the important targets in the PPI network by evaluating variables including degree, betweenness, and closeness. Using the DAVID database (**https://david.ncifcrf.gov/**), the KEGG enrichment pathway analysis and GO analysis of overlapping targets were carried out. The screening criteria for the chronic pharyngitis-related signaling pathways was p-value <0.05. The bioinformatics cloud platform (**https://www.bioinformatics.com.cn/**) was utilized to visualize the top 20 KEGG pathways and the top 10 GO terms. In the end, the "compound–target–pathway" (C–T–P) network was developed further to forecast core targets, active components, and putative BXHPD signaling pathways for the therapy of chronic pharyngitis.

Molecular docking verification

Following the PPI and C–T–P network screening of core targets and important effective components, molecular docking was carried out. The RCSB PDB database (**https://www.bioinformatics.com.cn/**) contains the 3D crystal structure of the core protein genes (receptors), such as AKT1 (PDB: 7MYX), MAPK1 (PDB: 6G54), MAPK3 (PDB: 6GES), EGFR (PDB: 7OM5), PIK3R1 (PDB: 6D81), RELA (PDB: 6NV2), PIK3CA (PDB: 7RRG), NFKB1 (PDB: 7LFC), and CCND1 (PDB: 6P8E). Additionally, PyMol 2.6.0 software was used to import the nine proteins and filter out organic and solvent molecules that weren't needed. Subsequently, ChemBio3D software was utilized to minimize energy and convert the 2D structures of the components (ligands) into Protein Data Bank (PDB) format. AutoDockTools 1.5.7 was used to preprocess the receptors and ligands. The visualization of the final conformation with the greatest affinity after AutoDock Vina 1.1.2 completed the receptor–ligand docking was acquired by PyMOL.

Molecular dynamics simulation (MDS)

A 100 ns MDS was achieved by Gromacs 2019.6 software.[19] Protein and ligand topology was generated with the AMBER99SB force field and the ACPYPE web server.[20,21] Dodecahedral boxes were designed using the SPC/E water model with a 1.0 nm margin. The system was neutralized using Na^+ or Cl^- ions. Energy minimization by the steepest descent method was followed by 40 ps of isothermal-isochoric (NVT) and 400 ps of isothermal isobaric (NPT). The temperature of the NVT and NPT equilibration was set at 300 K and the pressure was 1 bar. Five criteria were used to evaluate the stability of each complex: hydrogen bond number (HB), radius of gyration (R_g), root mean square fluctuation (RMSF), solvent accessible surface area (SASA), and root mean square deviation (RMSD). Lastly, the molecular mechanics Poisson–Boltzmann surface area (MMPBSA) method was devoted to calculating the binding energy between ligand and receptor.

Results

Determination and characterization of chemical profiles in BXHPD

Using UPLC-Q-Exactive Orbitrap-MS analysis, the chemical components in BXHPD were qualitatively identified. Thus, 121 components in total (12 lignans, 16 flavonoids, 51 organic acids, 19 alkaloids, 10 triterpenoids, 4 coumarins, 6 phenols, and 3 other-type components) were found in BXHPD extracts. Eight of these compounds could be positively identified by comparing their exact molecular weights and retention times to those of the reference standards. Fig. 2 displays the total ion chromatograms (TICs) of the BXHPD extracts in negative and positive ion modes. Fig. S1 (ESI†) displays the structures of 121 chemical components, and Table S1 (ESI†) provides a complete list of them.

Determination of lignans in BXHPD

Lignans are a class of naturally occurring compounds that are formed by polymerizing two molecules of phenylpropanoid derivatives (C6–C3 monomers), according to report.[18]

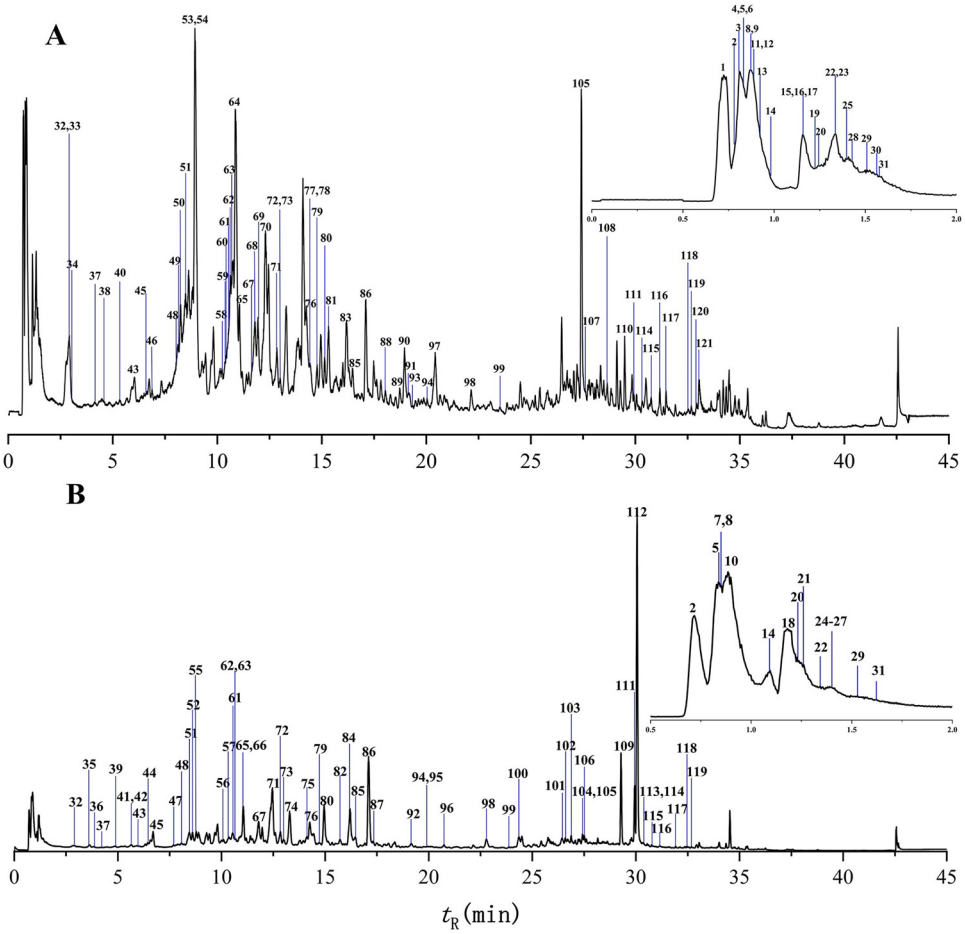

Fig. 2 The total ion chromatograms (TICs) of BXHPD extracts in positive and negative ion modes.

Hepatoprotective, neuroprotective, blood lipid-lowering, antioxidant, anti-tumor, and anti-inflammatory qualities are some of their pharmacological activities.[22,23] We have provisionally discovered twelve lignans that are created when two phenylpropanoids are connected by β,β′-carbon. The primary source of these lignans in BXHPD was *Magnolia officinalis* Rehd. et Wils. (HP). The benzene ring mother nucleus of lignans is relatively stable, and the possible cracking pathways are often the cleavage of side chain groups and dehydration.

At 29.28 min, compound **109** was discovered. It produced *m*/*z* 265.1234 $[M–H]^-$, revealing the elemental makeup of $C_{18}H_{18}O_2$. Furthermore, at *m*/*z* 249.0925, 224.0851, 223.0753, and 197.0605, the $[M–H]^-$ ion fractured into the distinctive ions $[M–H–CH_4]^-$, $[M–H–C_3H_5]^-$, $[M–H–C_3H_6]^-$, and $[M–H–C_3H_6–C_2H_2]^-$, respectively. Thus, compound **109** was identified as honokiol. Fig. 3A displays the associated secondary mass spectra and potential cleavage mechanism. The ion (*m*/*z* 265.1232 $[M–H]^-$) and the molecular formula ($C_{18}H_{18}O_2$) of compound **112** and compound **109** are identical. However, their cleavage pathways are very distinct from one another. In compound **112**, with a retention period of 30.05 min, *m*/*z* 247.1131 $[M–H–H_2O]^-$ was estimated *via* losing H_2O (18 Da), and *m*/*z* 223.0778 $[M–H–C_3H_6]^-$, inferred by losing C_3H_6 (42 Da). Thus, compound **112** was tentatively characterized as magnolol (Table S1, ESI†).

Determination of flavonoids in BXHPD

The fundamental skeleton of flavonoids is typically C6–C3–C6, with 2-phenylchromone serving as the mother nucleus. Flavonoids have anti-inflammatory, anti-tumor, hypoglycemic, hypotensive, neuroprotective, and anti-myocardial ischemia pharmacological effects.[24–26] The majority of naturally occurring flavonoids are found as oxygen glycosides, while a small number are found as carbon glycosides. The molecule readily loses its glucuronic acid (176 Da), glucose (162 Da), and rhamnosyl (146 Da) groups, when it is in the form of an oxygen glycoside, yielding the distinctive fragment ions $[M–H-176]^-$, $[M–H-162]^-$, and $[M–H-146]^-$. The sugar group is difficult to break directly when attached to a carbon glycoside bond; this results in the production of the distinctive fragment ions of $[M–H-120]^-$, $[M–H-60]^-$, and $[M–H-90]^-$. The cleavage mode of flavonoids and their glycosides has been thoroughly clarified, including the common cleavage behavior of saccharide cleavage and deglycosylation. Multiple neutral losses, including CO (28 Da), H_2O (18 Da), C_2H_2O (42 Da), and CO_2 (44 Da), as well as Retro Diels–Alder (RDA) cleavages, also produced the

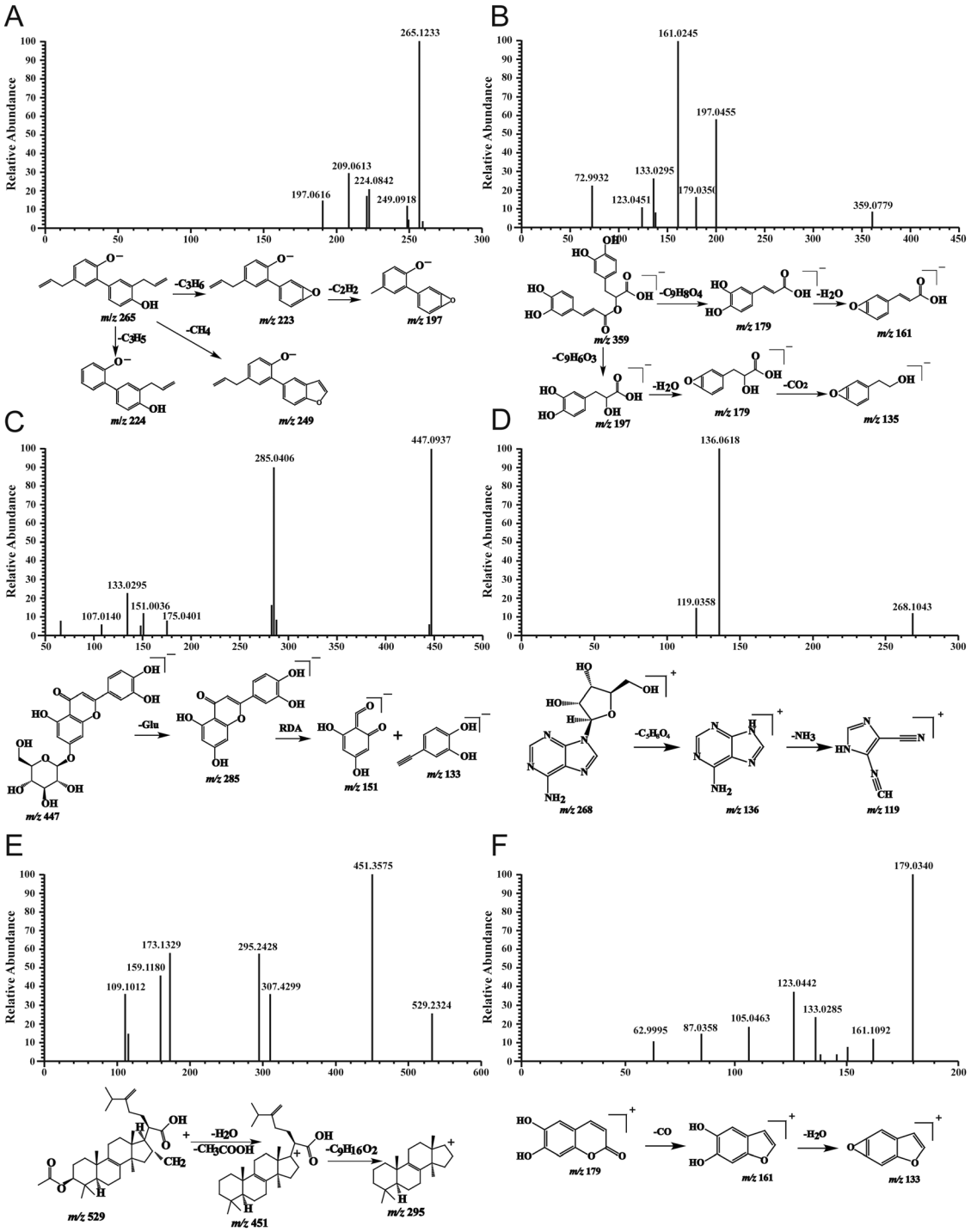

Fig. 3 The proposed fragmentation pathways of honokiol (A), luteolin-*O*-glucoside (B), rosmarinic acid (C), adenosine (D), pachymic acid (E), and esculetin (F).

characteristic ions.[27,28] In this study, 16 flavonoids including 9 flavones, 5 flavonols, 1 dihydroflavonol, and 1 flavanol were identified in BXHPD extracts, which all from HP and ZSY.

Compound **72** had an ion of *m*/*z* 447.0945 $[M–H]^-$ at 13.00 min, with the elemental makeup of $C_{21}H_{20}O_{11}$. Compound **72**'s MS/MS spectra and potential cleavage routes are displayed in Fig. 3C. The ion at *m*/*z* 285.0411 $[M–H–Glu]^-$ is the result of a glucose residue loss in MS/MS. The RDA cleavage then generated the ions at *m*/*z* 151.0038 and 133.0294. Notably, compound **72** was preliminarily inferred as luteolin-*O*-glucoside. Similarly, compound **94** showed *m*/*z* 285.0407 $[M–H]^-$ ion at 9.95 min, indicating that its chemical formula

is $C_{15}H_{10}O_6$. The RDA cleavage produced diagnostic ions, which were detected at *m*/*z* 151.0038 and 133.0294. Therefore, compound **94** was characterized as luteolin.

Determination of organic acids in BXHPD

The anti-inflammatory, antioxidant, and antibacterial effects of organic acids are significant.[29,30] The BXHPD found 51 different organic acids, comprising 22 phenylpropionic acids, 15 amino acids, and 14 other-type organic acids. These organic acids usually have hydroxyl, methoxy, and carboxyl groups in their structures. Thus, the neutral losses that were totaled were CO (28 Da), H_2O (18 Da), NH_3 (17 Da), HCOOH (46 Da), CH_3NH_2 (31 Da), and CO_2 (44 Da).

Compound **86** had an excimer ion of *m*/*z* 359.0774 $[M–H]^-$. It continuously lost $C_9H_6O_3$ (162 Da), H_2O (18 Da), and CO_2 (44 Da) to obtain *m*/*z* 197.0464 $[M–H–C_9H_6O_3]^-$, *m*/*z* 179.0350 $[M–H–C_9H_6O_3–H_2O]^-$, and *m*/*z* 135.0445 $[M–H–C_9H_6O_3–H_2O–CO_2]^-$, or continuously lost $C_9H_8O_4$ (180 Da) and H_2O (18 Da) to obtain *m*/*z* 179.0350 $[M–H–C_9H_8O_4]^-$ and *m*/*z* 161.0245 $[M–H–C_9H_8O_4–H_2O]^-$. Rosmarinic acid was assumed to be compound **86** based on comparison with ref. 31. Fig. 3B displays its MS/MS spectra as well as potential cleavage mechanisms. The same formula of $C_{16}H_{18}O_9$ ($[M–H]^-$, *m*/*z* 353.0869) was found in compounds **41**, **48**, and **55**, with different retention times. At *m*/*z* 179.0338 [caffeic acid–H]$^-$, 191.0559 [quinic acid–H]$^-$, and 135.0446 [caffeic acid–H–CO_2]$^-$, the fragment ions of them are same. Based on their relative peak intensities and retention times, compound **41** was determined as 5-*O*-caffeoyl quinic acid with compound **48** of 4-*O*-caffeoyl quinic acid, and compound **51** of 3-*O*-caffeoyl quinic acid.[32]

Determination of alkaloids in BXHPD

Six aporphine alkaloids, eight nucleoside and its base alkaloids, two benzyl tetrahydroisoquinoline alkaloids, and three other-type alkaloids were among the 19 alkaloid ingredients of BXHPD that were found. The typical fragmentation patterns for aporphine alkaloids included the breakage of the benzene ring side chain and the removal of the $(CH_3)_2NH$ (45 Da) and CH_3OH (32 Da) groups. Compound **64**, in particular, originated from a parent $[M]^+$ ion of *m*/*z* 342.1706. After removing the $(CH_3)_2NH$ group, *m*/*z* 297.1120 $[M–(CH_3)_2NH]^+$ was obtained. This generated diagnostic ions at *m*/*z* 265.0860 $[M–(CH_3)_2NH–CH_3OH]^+$ and *m*/*z* 237.0916 $[M–(CH_3)_2NH–CH_3OH–CO]^+$, which were implied by the constant loss of the CH_3OH (32 Da) and CO (28 Da) groups. Thus, it was concluded that compound **64** was magnoflorine.[33]

In this work, nucleoside and its base alkaloids are obtained from *Pinellia ternata* (Thunb.) Breit. (BX), and they can prevent vomiting and lessen negative reactions.[34] The ion at *m*/*z* 268.1043 $[M + H]^+$ ($C_{10}H_{13}N_5O_4$) was generated by compound **23**. Compound **23**'s mass spectrum showed the primary fragment ions, including *m*/*z* 136.0618 and *m*/*z* 119.0358. The fragment ion at *m*/*z* 136.0618 $[M + H–C_5H_8O_4]^+$ was assumed to have lost the $C_5H_8O_4$ (132 Da) group, indicating the D-ribosyl loss, which was formed by losing the amino group (17 Da) after ring opening and generated diagnostic ions at *m*/*z* 119.0358 $[M + H–C_5H_8O_4–NH_3]^+$. Compound **23** was assumed to be adenosine based on the cleavage rule of the standard and related literature.[35] Fig. 3D presented a proposal for the adenosine fragmentation pathway.

Determination of triterpenoids in BXHPD

Terpenoids' basic parent nucleus is composed of thirty carbon atoms. It is believed that the majority of triterpenoids are condensed from 6 isoprene. Triterpenoids have clear anti-inflammatory, antibacterial, antiviral, immunomodulatory, and anti-tumor effects.[36] Ten triterpenoids in all, all derived from *Poria cocos* (Schw.) Wolf (FL), were described in BXHPD in this work. Tetracycline triterpenoids. Triterpenes largely lost neutral molecules like CO (28 Da), H_2O (18 Da), and CH_3COOH (60 Da).

Compound **120** had an ion at *m*/*z* 529.2324 $[M + H]^+$, suggesting the chemical formula $C_{33}H_{52}O_5$. Compound **120** displayed *m*/*z* 451.3575 and *m*/*z* 295.2428 fragment ions. Of these, the ion at *m*/*z* 451.3575 $[M + H–H_2O–CH_3COOH]^+$ was thought to have lost the groups of H_2O (18 Da) and CH_3COOH (60 Da). By losing the $C_9H_{16}O_2$ (156 Da) group, it produced ions at *m*/*z* 295.2428 $[M + H–H_2O–CH_3COOH–C_9H_{16}O_2]^+$. Compound **120** was tentatively recognized as pachymic acid by the reference literature.[37] Fig. 3E shows the fragmentation route.

Determination of coumarins in BXHPD

Coumarins are divided into two categories: furanocoumarins and pyranocoumarins. Four pyranocoumarins were identified and characterized as a result of the current study. Coumarins share the same parent nucleus, benzene α-pyranone, while various side chain groups tend to be lost along with the loss of CO or CO_2 group in the lactone ring. Compound **49**, for instance, displayed the ion of $[M + H]^+$ at *m*/*z* 179.0342; its chemical composition was $C_9H_6O_4$. Its retention time was 8.15 min. The CO group loss produced the product ion at *m*/*z* 161.1092, which then proceeded to strip off the CO (28 Da) group or the H_2O (18 Da) group, obtaining fragments at *m*/*z* 123.0442 $[M + H–2CO]^+$ and *m*/*z* 133.0285 $[M + H–CO–H_2O]^+$. Consequently, compound **49** was deduced as esculetin, and possible cleavage pathways are shown in Fig. 3F.

Determination of phenols in BXHPD

SJ and ZSY are the sources of the phenol components found in BXHPD. Three of them are gingerols, which possess analgesic, antioxidant, anti-inflammatory, and cardiovascular function-improving properties.[38] At *m*/*z* 293.1767, compound **104** detected the precursor ion $[M–H]^-$, indicating that its chemical formula was $C_{17}H_{26}O_4$. After the $C_6H_{12}O$ and $C_{10}H_{10}O_4$ groups were eliminated, the distinctive ions of *m*/*z* 193.0878 $[M–H–C_6H_{12}O]^-$ and *m*/*z* 99.0798 $[M–H–C_{10}H_{10}O_4]^-$ were found, and *m*/*z* 57.0348 $[M–H–C_6H_{12}O–C_8H_8O_2]^-$ was created by further losing the $C_8H_8O_2$ group by *m*/*z* 193.0878. In light of this, compound **104** was provisionally determined to be 6-gingerol using the reference standard.

Characterization of prototype and metabolic components

It is particularly challenging to detect exogenous components in complex biological matrixes because of endogenous components and background noise. By employing the control sample data set as the background, background reduction could uncover prototype and metabolite peaks.[39] The background subtraction method used in this work is intended to improve identification efficiency by specifically subtracting interfering ions from the entire mass spectrum. Fig. S2 (ESI†) displays the background-subtracted ion chromatograms (TICs) and TICs of the exogenous component of plasma samples in both positive and negative modes. We first identified or preliminary described 50 types of exogenous components (including 23 prototypes and 27 metabolites) from BXHPD in rat plasma following the data processing technique. The extract ion chromatograms of the 27 metabolites are shown in Fig. 4.

We identified or roughly characterized 23 prototype components in rat plasma samples based on retention time, precise molecular weights, and mass fragmentation of components in BXHPD extracts. These components included 7 organic acids, 5 lignans, 4 alkaloids, 3 flavonoids, 2 phenols, and 2 coumarins. Table S2 (ESI†) presents the comprehensive MS fragmentation data. The absorbed prototypes may travel *via* the phase I metabolic pathway, which could expose or add polar groups. These compounds conjugate with glucuronic acid, sulfuric acid, or other molecules to improve water solubility and enable excretion, which is followed by the phase II metabolic pathway.[40]

Table S3 (ESI†) illustrates the identification or provisional characterization of a total of 27 metabolites derived from the chemical compound information found in BXHPD and the suggested metabolic pathways. Phase I reactions of hydrogenation, hydroxylation, and demethylation, as well as phase II reactions of conjugating with sulfuric acid or glucuronic acid, are the principal metabolic reactions of the prototype components. Fig. 5 displays the suggested metabolic pathways for the representative components.

Characterization of metabolites from lignan

Rat plasma contained 12 metabolites from lignans, including two randaiol, one magnolignan A, one randainol, five magnolol, and two honokiol-related metabolites. At 26.67 min, compound **M23** was discovered. It produced *m*/*z* 441.1554 $[M-H]^-$ with the elemental makeup of $C_{24}H_{26}O_8$. At *m*/*z* 265.1225, 249.0921, 224.0838, and 197.0613, the $[M-H]^-$ ion fractured into the distinctive ions $[M-H-GluA]^-$, $[M-H-GluA-CH_4]^-$, $[M-H-C_3H_6]^-$, and $[M-H-GluA-C_5H_8]^-$, respectively. By comparing the mass fragmentation behaviors of magnolol (Fig. 3A) and ref. 41, compound **M23** was identified as honokiol-*O*-

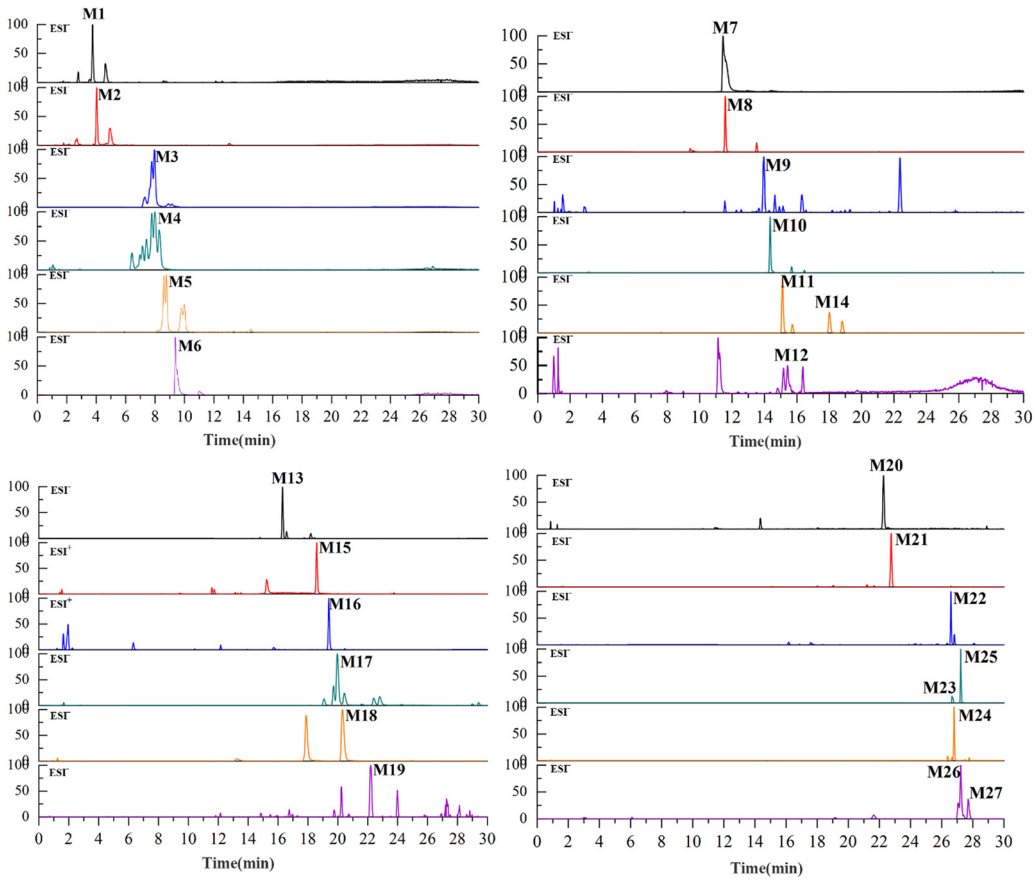

Fig. 4 Extract ion chromatograms (EICs) of the 27 metabolites after oral administration of BXHPD in negative and positive modes.

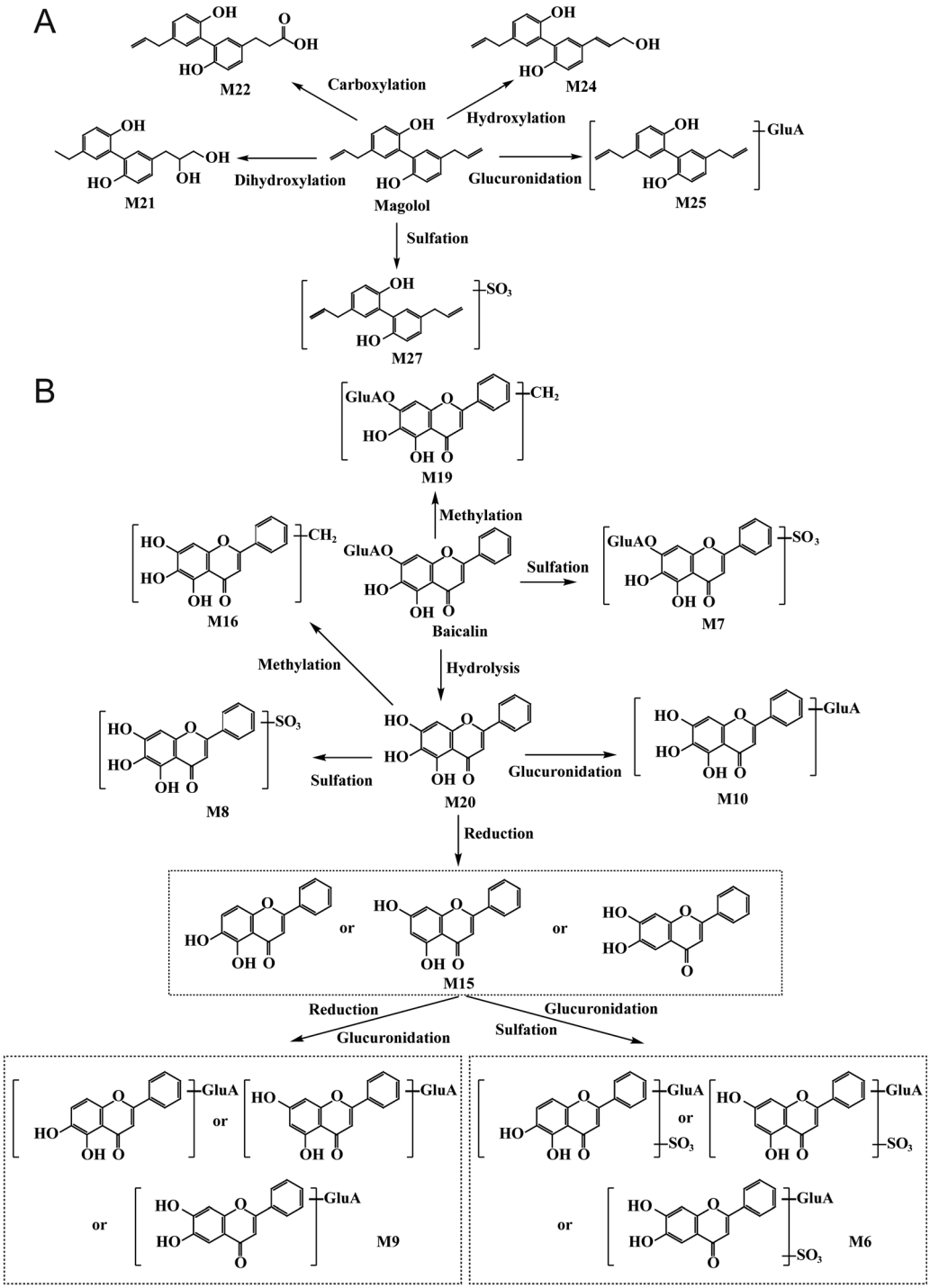

Fig. 5 Possible metabolic pathways of magnolol (A) and baicalin (B) in rats.

glucuronide. Fig. S3A (ESI†) displays the associated secondary mass spectra and potential cleavage mechanism.

The hydroxylation, carboxylation, sulfation, and glucuronidation metabolic pathways were among them. For instance, a $[M–H]^-$ ion at *m*/*z* 297.1145 ($C_{18}H_{16}O_4$) was generated by the metabolite **M22**, with 32 Da greater than magnolol (P23). Magnolilol's MS/MS spectra showed a neutral loss fragment of 44 Da, which produced the $[M–H–CO_2]^-$ ion with *m*/*z* 253.0875, showing the existence of a carboxyl group. By analyzing the mass fragmentation behaviors of magnolol, it was possible to identify **M22** as a carboxylated magnolol derivative. The dihydroxylation and hydroxylation products of magnolol were identified as **M21** ($C_{18}H_{20}O_4$, 34 Da higher than magnolol) and **M24** ($C_{18}H_{18}O_3$, 16 Da higher than magnolol) using the same inference thinking. The glucuronidation and sulfation products of magnolol could be assumed to be **M25**

($C_{24}H_{26}O_8$, 176 Da higher than magnolol) and **M27** ($C_{18}H_{18}O_5S$, 80 Da higher than magnolol) (Fig. 5A).

Characterization of metabolites from flavonoid

Nine metabolites from flavonoids in all, all derived from baicalin (P15), were found. Baicalin underwent several metabolic changes, including methylation, hydrolysis, reduction, glucuronidation, and sulfation. Compound **M19** had a $[M–H]^-$ ion at *m*/*z* 461.1077, which was more CH_2 (methylene unit) than that of baicalin and corresponded to the chemical formula $C_{22}H_{22}O_{11}$. Further evidence for a glucose moiety (176 Da) loss was provided by the distinctive ion of *m*/*z* 285.0772 $[M–H–GluA]^-$. Consequently, it was hypothesized that **M19** was baicalin's methylation product. At *m*/*z* 525.0350 ($C_{15}H_{10}O_8S$), **M7** displayed a quasi-molecular ion $[M–H]^-$, which was 80 Da (SO_3) more than baicalin. Additionally, fragment ions were produced at *m*/*z* 445.0792 $[M–H–SO_3]^-$, 349.0024 $[M–H–GluA]^-$, and 269.0453 $[M–H–SO_3–GluA]^-$. **M7** was thus recognized as the sulfated byproduct of baicalin. **M20** was found to be a hydrolyzed derivative of baicalin, having a molecular weight of 176 Da less than baicalin's. Metabolites **M16**, **M8**, **M15**, and **M10** were produced *via* the methylation, sulfation, reduction, and glucuronidation of **M20**, respectively. Moreover, **M15** was reduced and glucuronidated, which resulted in the creation of **M9**. **M16** was created concurrently with the glucuronidation and sulfation of **M15**. Fig. 5B shows the metabolic pathways that have been suggested.

Characterization of metabolites from organic acid

This investigation found 5 metabolites generated by organic acid, which were sulfates generated by combining one molecule of SO_3 with organic acids. Syringic acid-*O*-SO_3 (**M1**), vanillic acid-*O*-SO_3 (**M2**), *p*-coumaric acid-*O*-SO_3 (**M3**), caffeic acid-*O*-SO_3 (**M4**), and ferulic acid-*O*-SO_3 (**M5**) were the names given to these five metabolites. These five metabolites were found to have common fragment ions $[M–H–SO_3]^-$ and $[M–H–CO_2]^-$. These ions were generated by losing one molecule of SO_3 (80 Da) and one molecule of CO_2 (44 Da), respectively. For instance, at *m*/*z* 273.0073 ($C_{10}H_{10}O_7S$), **M5** displayed an ion of $[M–H]^-$ that was 80 Da more than ferulic acid. **M5** fragmented in a manner resembling that of ferulic acid, producing fragment ions at *m*/*z* 193.0505 $[M–H–SO_3]^-$, *m*/*z* 178.0272 $[M–H–SO_3–CH_3]^-$, *m*/*z* 149.0609 $[M–H–SO_3–CO_2]^-$, and *m*/*z* 134.0373 $[M–H–SO_3–CH_3–CO_2]^-$ (Table S3, ESI†). **M5** was therefore identified as a ferulic acid sulfation product.[42] Fig. S3B (ESI†) displays the associated secondary mass spectra and potential cleavage mechanism.

Identification of potential targets of BXHPD against chronic pharyngitis

Components entering the blood, such as prototype and metabolic molecules, were thought to be a potentially effective part of BXHPD. Therefore, the effective components of BXHPD against chronic pharyngitis and its mechanism of action were screened by the network pharmacology method driven by absorption components. Consequently, by overlapping 1401 chronic pharyngitis-related targets and 662 absorbed components-related targets, 208 common targets were found. The Venn diagram is displayed in Fig. 6A. It was discovered that these 208 targets could be effective therapeutic targets for BXHPD against chronic pharyngitis.

GO and KEGG enrichment analysis

GO items in all, comprise 911 biological processes, 186 molecular functions, and 112 cell components ($p < 0.05$). The top 10 important GO entries were displayed in Fig. 6E. Biological process was mainly related to response to xenobiotic stimulus, positive regulation of MAPK cascade, protein phosphorylation, and peptidyl–tyrosine phosphorylation, *et al.* KEGG pathway analysis of 208 common targets also revealed that 179 pathways related to BXHPD treatment of chronic pharyngitis were enriched ($p < 0.05$). The top 20 important KEGG pathways are displayed in Fig. 6D. After a comprehensive literature search, it is found that PI3K-Akt, MAPK and TNF signaling pathways are potentially important and feasible ways for BXHPD to treat chronic pharyngitis.

Core targets and potential effective components screening

Utilizing the PPI network and C–T–P network analysis, the screening process for potential effective components and core targets was finished. The PPI network was built and shown in Fig. 6B. Twenty-five highly linked targets were found using the PPI network's topological parameters filtering (Fig. 6C). Besides, plasma migrant components, the important KEGG pathways (Fig. 6D), and the related targets in BXHPD were involved in the construction of the C–T–P network (Fig. 7A). Randainol-*O*-sulfate, dihydroxydihydromagnolol, magnolignan A, carboxylated magnolol, magnoflorine, hydroxylated magnolol, apigenin, honokiol, magnolol, and randainal that have a degree greater than 18 were ranked among the top ten ingredients and were considered to be potentially effective components of BXHPD in treating chronic pharyngitis (Fig. 7B). In the meantime, two gene sets overlapped in the intersection diagram (Fig. 7C) between the top 20 targets by the degree in the C–T–P network and the 25 highly related targets in the PPI network. There were nine core targets found: EGFR, PIK3R1, RELA, PIK3CA, NFKB1, AKT1, MAPK1, MAPK3, and CCND1.

Molecular docking validation and effective components further screening

The ten potential components and nine core targets were docked molecularly. The binding affinities of the molecular docking results are displayed in Fig. 7D. All ten components (ligands) showed binding energies of ≤ -5.3 kcal mol^{-1} with the receptors, which demonstrated strong binding affinities between the core target proteins and the potential effective constituents of BXHPD. The best affinity modes of nine core targets are CCND1-magnoflorine (-7.0 kcal mol^{-1}), NFKB1-magnoflorine (-6.7 kcal mol^{-1}), PIK3CA-apigenin (-7.5 kcal mol^{-1}), RELA-honokiol (-7.6 kcal mol^{-1}), PIK3R1-randainal (-5.8 kcal mol^{-1}), EGFR-magnolignan A (-7.3 kcal mol^{-1}), MAPK3-apigenin (-8.6 kcal mol^{-1}), MAPK1-magnolignan A (-7.1 kcal mol^{-1}), and AKT1-apigenin

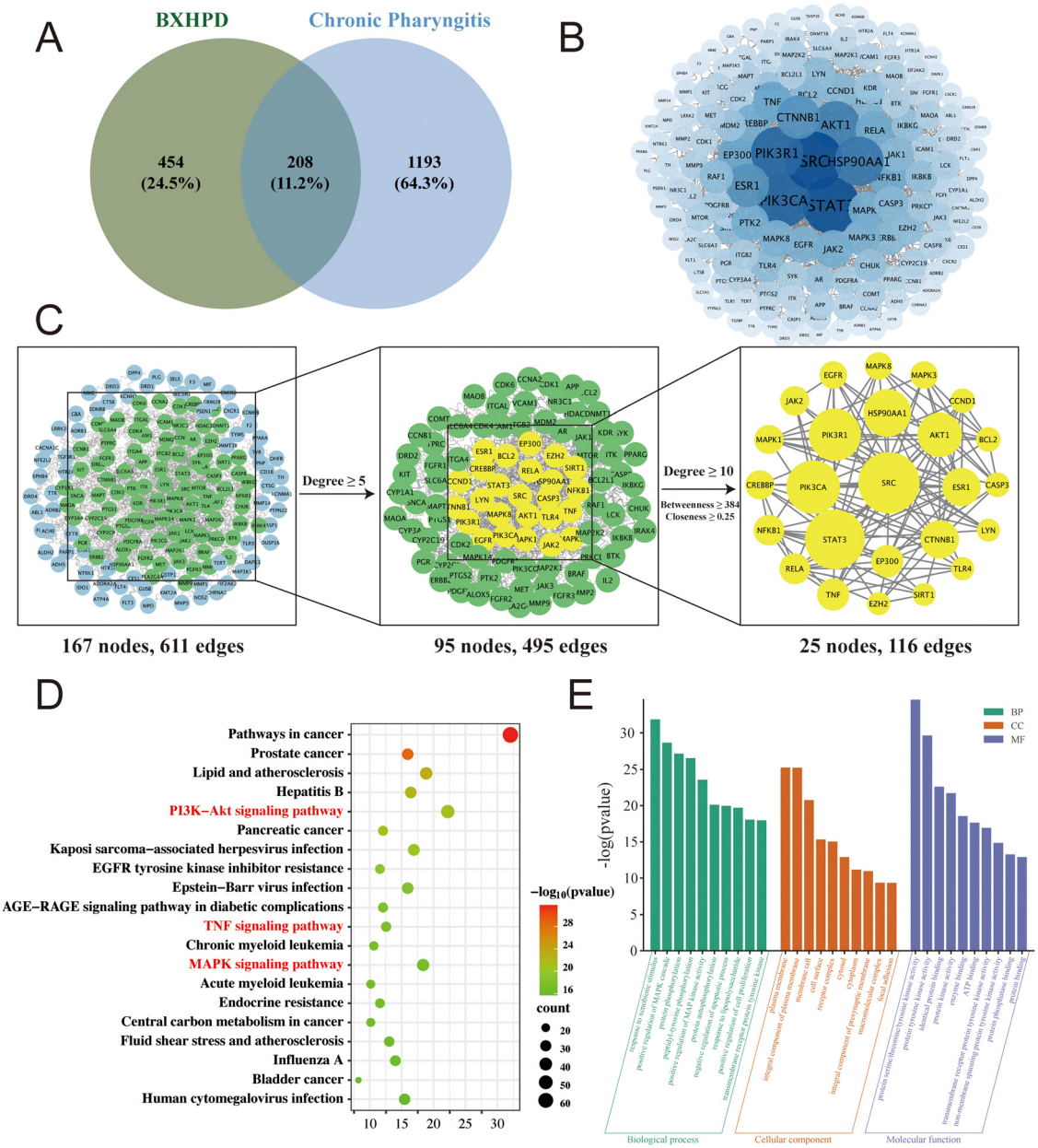

Fig. 6 Network pharmacology results of BXHPD against chronic pharyngitis. (A) Venn diagram of the intersection of the targets between BXHPD and chronic pharyngitis. (B) PPI network of 208 common targets. Each node represents a protein. Edges represent interactions between nodes. The color and size of each node represent the degree value, the darker the color, the larger the node, indicating the larger the degree value. (C) Screening of key targets by relative topological parameters. (D) KEGG pathway enrichment analysis of 208 common targets. The top 20 pathways are listed based on the *p* values. Node size is based on gene ratio, node color is based on −log(*p*) value. (E) GO enrichment analysis terms of 208 common targets. The top 10 terms of biological process, cellular component, and molecular function are displayed.

(−6.9 kcal mol^{-1}) complexes. Among these, magnolignan A, randainal, apigenin, honokiol, and magnoflorine are crucial to the outcomes of molecular docking. As a result, the five elements are thought to be BXHPD's potent ingredients for treating chronic pharyngitis.

Pymol 2.6.0 was used to visualize the hypothesized chemical mechanism of the top nine complexes to investigate their intermolecular force, as shown in Fig. 8. Hydrogen bonds were primarily responsible for the development of stable small molecule complexes, as well as the formation of active cavities for proteins. For instance, the results showed that apigenin can engage through three hydrogen bonds with the MAPK3 residues ARG-844 and GLY-186. Magnolignan A can form three hydrogen bonds with SER-246, SER-248, and ASP-251 residue in MAPK1. Randainal could bind to the residue of THR-296 and GLU-297 in PIK3R1 with four hydrogen bonds.

Molecular dynamics simulation (MDS) results

In order to explore the fluctuations and conformational changes that occur during receptor–ligand interaction, the

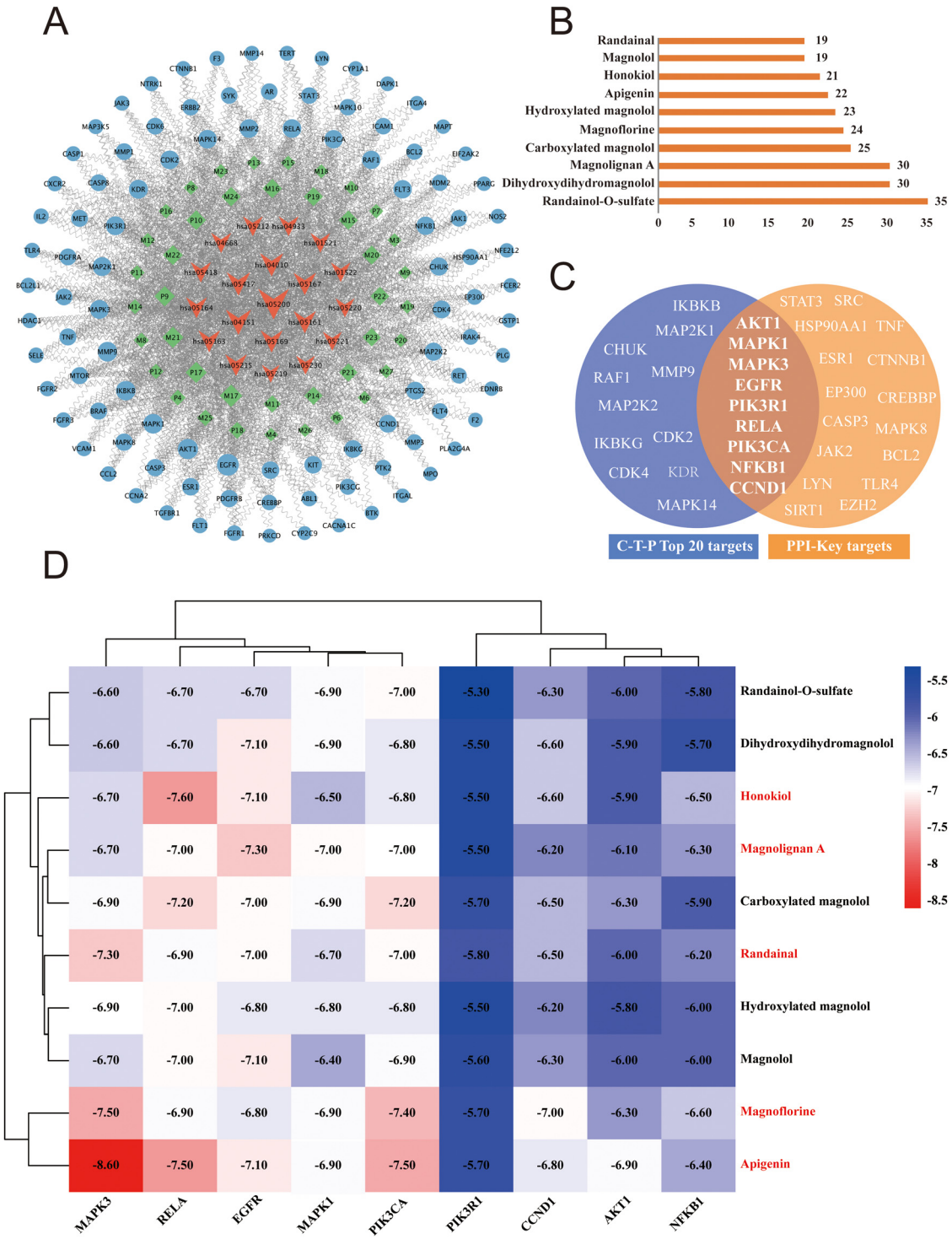

Fig. 7 (A) Network diagram of compound–target–pathway. (B) Top ten components in the compound–target–pathway network with degree values. (C) Venn diagram of 25 highly connected targets in PPI network and the top 20 targets of degree in compound–target–pathway network. (D) Results of molecular docking. The redder the color, the smaller the corresponding value, indicating the greater the docking strength.

100 ns MDS was used to examine the binding stability of PIK3CA-apigenin (−7.5 kcal mol^{-1}), RELA-honokiol (−7.6 kcal mol^{-1}), EGFR-magnolignan A (−7.3 kcal mol^{-1}), and MAPK3-apigenin (−8.6 kcal mol^{-1}) complexes. Utilizing the RMSD/RMSF/SASA/R_g analysis, the dynamic trace of the four complexes was investigated. Based on the RMSD data, it was found that both of the four complexes maintained stability in the simulated system with smooth oscillations within a specific range (Fig. 9A). Furthermore, improved stability is indicated by a lower RMSD value. The four complexes exhibited

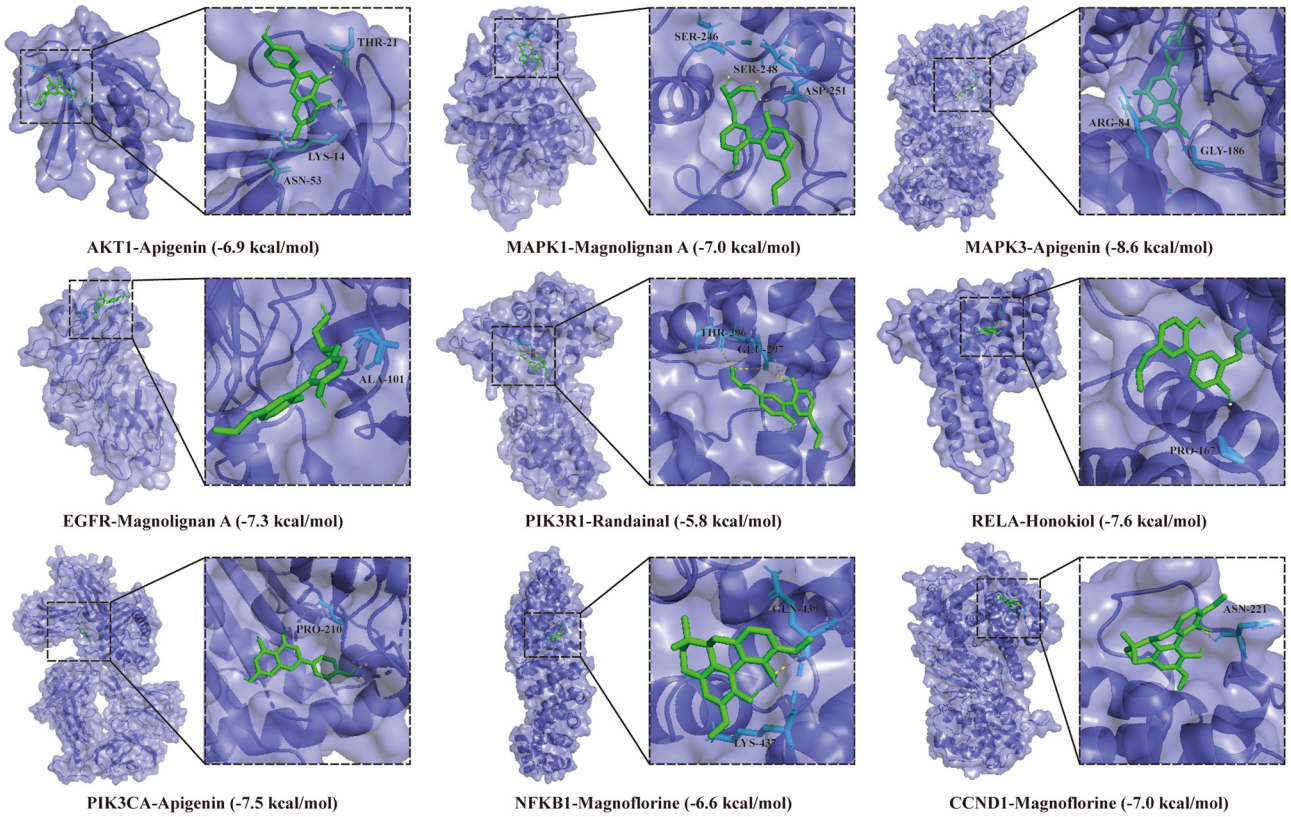

Fig. 8 The best docking patterns of the core target proteins and compounds. The purple represents the surface and cartoon style of protein receptors, green represents small molecule ligands, blue represents receptor residues, and yellow represents hydrogen bonds.

comparable atomic fluctuations. Specifically, the PIK3CA-apigenin complex (1.2 Å) demonstrated greater stability compared to EGFR-magnolignan A (1.4 Å), whereas MAPK3-apigenin (1.7 Å) outperformed RELA-honokiol (2.2 Å). Using RMSF analysis, we can understand how important residues vary over the MDS. The RMSF of every protein residue throughout the MDS of the four component-protein complexes is shown in Fig. 9B. Compared to EGFR-magnolignan A and PIK3CA-apigenin complex, the RMSF values of MAPK3-apigenin and RELA-honokiol complex show a more pronounced variation. The outcome is in line with the RMSD. SASA is a measure of protein hydrophobicity; a lower SASA value indicates a lesser likelihood of coming into contact with water molecules. The SASA values for MAPK3-apigenin and EGFR-magnolignan A complex were calculated as 1450 Å^2 and 870 Å^2, and the other two complexes had similar values near 700 Å^2 (Fig. 9C). R_g can be used to evaluate the compactness of the protein structure. The R_g value is lower, the protein structure is more stable. As shown in Fig. 9D, the R_g values of the four complexes do not significantly change, indicating that the complexes stay stable throughout the simulation. The R_g values of EGFR-magnolignan A were approximately 14.7 Å, PIK3CA-Apigenin and RELA-Honokiol were close at 13.2 Å, and MAPK3-apigenin was approximately 19.1 Å. Our hydrogen bond analysis results (Fig. 9E) demonstrated that these complexes' hydrogen bond numbers were kept constant at 1–3 throughout the MDS, demonstrating their strong binding affinity. The MMPBSA approach elucidates the contributions of several energies, such as electrostatic (E_{ELE}), polar solvation (E_{PS}), van der Waals force (E_{VDW}), and SASA (E_{SASA}). It was discovered that E_{VDW} contributed more to the process of protein–ligand binding than did other types of energy. The four complexes' binding abilities are as follows: MAPK3-apigenin > RELA-honokiol > PIK3CA-apigenin > EGFR-magnolignan A.

Discussion

Although the BXHPD prescription is a well-researched clinical intervention for chronic pharyngitis, its broad applicability is limited by the lack of clarity surrounding its material foundation and underlying mechanism. The chemical composition of TCM prescriptions is a vital component that primarily contributes to their efficacy as a treatment. Therefore, it becomes essential to decipher BXHPD's complete molecular composition. In this study, 121 components were found in BXHPD extracts by UPLC-Q-Exactive Orbitrap-MS, including 12 lignans, 16 flavonoids, 51 organic acids, 19 alkaloids, 10 triterpenoids, 4 coumarins, 6 phenols, and 3 other-type components. Among them, 8 compounds were unambiguously identified through the comparison with the mass fragmentation behaviors and retention time of reference standards. Recently, Wang *et al.*[15]

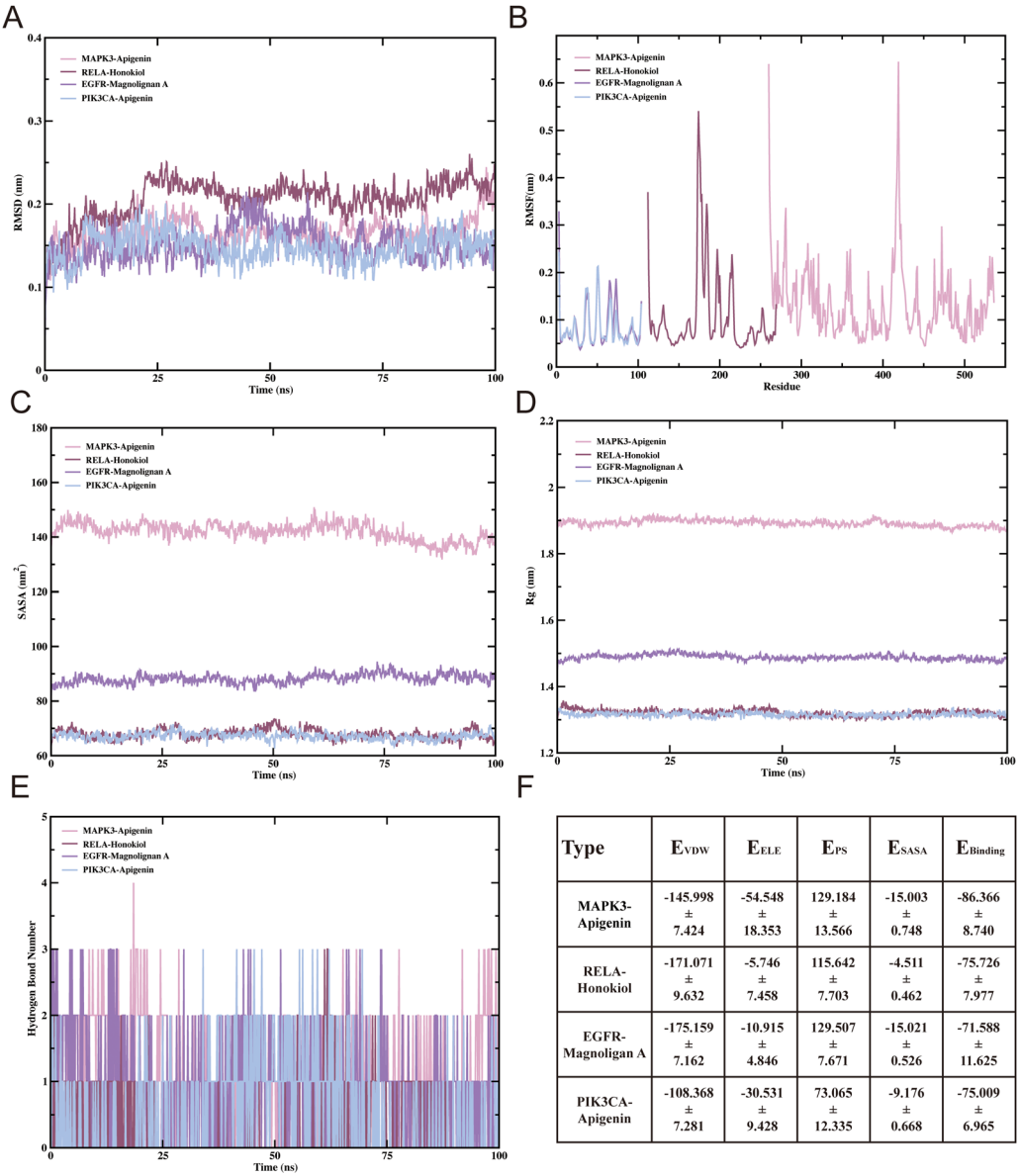

Type	E_{VDW}	E_{ELE}	E_{PS}	E_{SASA}	$E_{Binding}$
MAPK3-Apigenin	-145.998 ± 7.424	-54.548 ± 18.353	129.184 ± 13.566	-15.003 ± 0.748	-86.366 ± 8.740
RELA-Honokiol	-171.071 ± 9.632	-5.746 ± 7.458	115.642 ± 7.703	-4.511 ± 0.462	-75.726 ± 7.977
EGFR-Magnoligan A	-175.159 ± 7.162	-10.915 ± 4.846	129.507 ± 7.671	-15.021 ± 0.526	-71.588 ± 11.625
PIK3CA-Apigenin	-108.368 ± 7.281	-30.531 ± 9.428	73.065 ± 12.335	-9.176 ± 0.668	-75.009 ± 6.965

Fig. 9 The results of molecular dynamics simulation. The RMSD (A), RMSF (B), SASA (C), R_g (D), and Hbond (E) of PIK3CA-apigenin, RELA-honokiol, EGFR-magnolignan A, and MAPK3-apigenin complexes. (F) The binding energy is calculated by MMPBSA (kJ mol^{-1}).

identified 128 nonvolatile compounds and 145 volatile compounds in BXHPD samples combining UHPLC-QTOF-MS, HS-SPME-GC-MS, and HS-GC-IMS. Compared with this previous work, **83** compounds were identified for the first tine using UPLC-Q-Exactive Orbitrap-MS analysis in our study, only **38** of **121** compounds were the same as those found in earlier work. Origin, harvesting period, storage conditions, detecting instruments, and processing techniques are some of the elements that contribute to the discrepancy.[43]

According to the principles of plasma pharmacochemistry, potential active ingredients could be related metabolites or bloodstream-absorbing prototypes.[44] In the meanwhile, knowledge of the *in vivo* metabolic pathways of BXHPD was advanced through the identification of prototypes and metabolites in plasma. Our research preliminarily characterized 50 kinds of exogenous components including 23 prototypes and 27 metabolites from plasma samples of rats treated with BXHPD. The main metabolic pathways of the prototype components include phase I reactions of hydroxylation, hydrogenation, and demethylation, phase II reactions of conjugating with sulfuric acid or glucuronic acid. These findings served as a foundation for deciphering the pharmacodynamic material basis of BXHPD.

Network pharmacology follows the holistic approach of TCM treatment by examining the relationships between targets, components, signal pathways, and illnesses. It has been widely utilized to forecast the primary active substances and potential targets of TCM prescriptions. In this research, the results of PPI and C–T–P networks revealed the nine core target genes, which were EGFR, PIK3R1, RELA, PIK3CA, NFKB1, AKT1, MAPK1,

MAPK3, and CCND1. The anti-inflammatory effects may be either directly or indirectly relevant to these core target genes. The NF-κB pathway plays a major regulatory role in the expression of genes associated with inflammation, and the transcription factors RELA and NFKB1 are members of this family.[45] The survival factor AKT1 can suppress the pro-inflammatory factors TLR4 and NF-κB.[46] NLRP3 plays a crucial role in inflammation, and NLRP3 inflammasome signaling pathway activation may be inhibited by hindering the PI3K-Akt pathway.[47] Numerous cellular functions, including as apoptosis, proliferation, inflammation, and innate immunity, are regulated by MAPKs (mitogen-activated protein kinases).[48] Among the major members of MAPKs found in mammals are ERK, p38 MAPK, and JNK. In the MAPK/ERK cascade, MAPK1 and MAPK3 are crucial. One member of the ErbB receptor family, EGFR, is a crucial hub engaged in several pathways, such as PI3K-Akt, JAK2/STAT, and RAS/MAPK signaling, which is partially mediated by its activation and autophosphorylation.[49]

Acute pharyngitis repeated attacks or upper respiratory tract infections brought by *Streptococcus pneumoniae*, *Staphylococcus aureus*, and group A β-hemolytic *Streptococcus*, can result in chronic pharyngitis.[50] The findings of network pharmacology, MDS, and molecular docking in this investigation discovered and validated the binding properties of five key compounds, that is, magnoflorine, apigenin, honokiol, randainal, and magnolignan A to nine core proteins targets. The five ingredients, which could be recommended as effective components of BXHPD against chronic pharyngitis, displayed varying degrees of anti-inflammatory and antibacterial properties through regulating the PI3K-Akt, TNF, and MAPK signaling pathways. Magnoflorine is a quaternary aporphine alkaloid, which may have a significant anti-inflammatory impact by preventing the process of producing nitric oxide (NO).[51] Guo *et al.*[52] proved that the expression of multiple cytokines (IL-6, TNF-α, and IL-1β) was dose-dependently reduced by magnoflorine. The suppression of MAPK signaling pathways is one of the potential mechanisms for this effect. Apigenin, a naturally occurring phyto-flavonoid, has been reported to prevent p38, ERK, and JNK pathway phosphorylation,[53] inhibit the production of COX-2 by preventing Akt signal transduction,[54] and modulate TNF-α, IL-2, IL-1β, IL-6, and IL-8 factors,[55] thus exerting its anti-inflammatory action.[56] Song *et al.*[57] showed that apigenin could reduce the pathogenicity of *Streptococcus pneumoniae*. Honokiol, a natural biphenyl neolignane, could modulate the NF-κB or MAPK pathway to suppress the release of TNFα and NO,[58,59] regulate the phosphorylation of the JNK, p38, PI3K-Akt, and ERK1/2 pathway,[60] and inhibit the priming and activation stages of the NLRP3 inflammasome.[61] Some reports demonstrated that honokiol showed effective antibacterial and antibiofilm activity while damaging the membrane and cell wall of *Staphylococcus aureus.*[62]

The need for pharmacokinetic characteristics of medications is growing as pharmacochemistry advances. Nowadays, a drug's pharmacokinetic qualities are just as important as its effectiveness and low toxicity when evaluating its drug-forming qualities and potential applications.[63] Xue *et al.*[64] found that the mean time to peak concentration (T_{max}), mean residence time (MRT), half-life ($T_{1/2}$), and clearance (CL) of magnoflorine in rats were 1.13 h, 4.92 h, 1.52 h, and 61.34 L h^{-1} kg^{-1}, respectively. Other studies have also shown that magnoflorine had high absorption, low bioavailability, and low elimination rates.[65,66] The pharmacokinetic correlation of apigenin lies in that it determines how much apigenin can be used by human intestinal microflora by oral intake. Apigenin's oral bioavailability is demonstrated to be low; it is either quickly metabolized after absorption or eliminated unabsorbed in the urine or feces.[67] Honokiol demonstrates a biphasic kinetic profile, consisting of a rapid distribution phase followed by a slower elimination phase.[68,69] Furthermore, after intravenous treatment in animal models, the pharmacokinetic profile of honokiol has demonstrated a favorable spectrum of bioavailability, making it a potential agent for clinical trials. Thus, the pharmacokinetics study of these key components will be the important direction of our future research.

The safeguarding impact of BXHPD against chronic pharyngitis was mostly attributed to anti-inflammatory and antibacterial actions, as demonstrated by the previously described data. There were certain restrictions on this investigation. Firstly, the inherent bias in databases is a common issue in the field of network research, which still heavily relies on them. Our investigation's results may be particularly impacted by the database's timeliness and completeness. Future network analysis research should aim to continuously develop and update databases with timely information to reduce these biases. The integration of MDS and molecular docking technologies has increased the accuracy of the network prediction. However, the protein levels of the screened core targets still need further verification by *in vivo* experiments. Furthermore, more investigation is required to ascertain how the five potentially beneficial ingredients that were evaluated for antibacterial and anti-inflammatory properties interact with one another. To get over these restrictions, we want to conduct more *in vivo* and *in vitro* investigations to look into the possible active components and associated mechanisms of BXHPD against chronic pharyngitis.

Conclusion

In order to determine the pharmacodynamic material foundation of BXHPD in the treatment of chronic pharyngitis and assess potential molecular pathways, this work established a sensitive and rapid UPLC-Q-Exactive Orbitrap-MS technology in conjunction with network pharmacology. Finally, **121** components were preliminarily identified in BXHPD extracts including 12 lignans, 16 flavonoids, 51 organic acids, 19 alkaloids, 10 triterpenoids, 4 coumarins, 6 phenols, and 3 other-type components. Moreover, plasma samples from rats given BXHPD were used to qualitatively assess 50 exogenous components, comprising 23 prototypes and 27 metabolites. The integrated analysis showed that five effective components (magnoflorine, apigenin, honokiol, randainal, and magnolignan A), nine core targets (EGFR, PIK3R1, RELA, PIK3CA, NFKB1, AKT1, MAPK1,

MAPK3, and CCND1), and three signaling pathways (PI3K-Akt, TNF, and MAPK signaling pathways) might be vital. The BXHPD might display multiple mechanisms of anti-inflammatory and antibacterial properties against chronic pharyngitis. In parallel, molecular docking and MDS validated the binding properties of key compounds to the core targets. In summary, the findings might provide a foundation for further research on quality assurance and the therapeutic use of BXHPD to treat chronic pharyngitis. However, additional research involving animal experiments is required to confirm and validate the above-mentioned beneficial ingredients, core targets, and signaling pathways.

Abbreviations

BXHPD	Banxia Houpo Decoction
TCM	Traditional Chinese medicine
UPLC-Q-Exactive Orbitrap-MS	Ultra-high performance liquid chromatography coupled with a Q exactive hybrid quadrupole-orbitrap mass spectrometry
TIC	Total ion chromatography
EICs	Extract ion chromatograms
KEGG	Kyoto encyclopedia of genes and genomics
PPI	Protein–protein interaction
MAPK1	Mitogen-activated protein kinase 1
AKT1	RAC-alpha serine/threonine-protein kinase
EGFR	Epidermal growth factor receptor
MAPK3	Mitogen-activated protein kinase 3
PIK3R1	Phosphatidylinositol 3-kinase regulatory subunit alpha
RELA	Transcription factor p65
PIK3CA	Phosphatidylinositol 4,5-bisphosphate 3-kinase catalytic subunit alpha isoform
NFKB1	Nuclear factor NF-kappa-B p105 subunit
CCND1	G1/S-specific cyclin-D1
MDS	Molecular dynamics simulation
SASA	Solvent accessible surface area
R_g	Radius of gyration
RMSD	Root mean square deviation
HB	Hydrogen bond number
RMSF	Root mean square fluctuation
MMPBSA	Molecular mechanics Poisson–Boltzmann surface area.

Author contributions

Yanru Liu: Conceptualization, performed the experiments, data curation, formal analysis, visualization, validation, writing – original draft. Jiayi Zheng: data curation, formal analysis, visualization. Lu Shen: conceptualization, performed the experiments, data curation, visualization. Gongjun Yang: conceptualization, supervision, writing – review & editing. Fang Feng: conceptualization, funding acquisition, project administration, supervision, validation, writing – review & editing.

Data availability

The authors confirm that the data supporting the findings of this study are available within the article and/or its ESI.†

Conflicts of interest

The authors declare that none of the work reported in this study could have been influenced by any known competing financial interests or personal relationships.

Acknowledgements

The National Natural Science Foundation of China (numbers 81872993, 30973858) provided funding for this work.

References

1 J. O. Kumari and R. Rajendran, *Indian J. Otolaryngol Head Neck Surg.*, 2008, **60**, 199–201.
2 R. C. Murray and S. K. Chennupati, *Infect. Disord.: Drug Targets*, 2012, **12**, 281–285.
3 L. Chen, Y. Lai, L. Dong, S. Kang and X. Chen, *Microb. Pathog.*, 2017, **113**, 365–371.
4 C. Y. Xu, R. S. Yue, X. L. Lv, T. C. Wu, M. Y. Yang and Y. Chen, *Medicine*, 2020, **99**(30).
5 Z. C. Li, J. L. Huang and Z. P. Hu, *Int. J. Environ. Res. Public Health*, 2019, **16**, 1688.
6 F. Ran, X. Han, X. Deng, Z. Wu and L. Han, *Biomed. Pharmacother.*, 2021, **140**, 111787.
7 M. Kostic, M. Ivanov, S. S. Babic, J. Petrovic, M. Sokovic and A. Ciric, *Curr. Med. Chem.*, 2020, **27**, 6892–6909.
8 C. Li, F. Wu, W. Yuan, Q. Ding, M. Wang, Q. Zhang, J. Zhang, J. Xing and S. Wang, *J. Evidence-Based Complementary Altern. Med.*, 2019, **2019**, 9458676.
9 R. Yoshinaga, T. Maki, Y. Goto, H. Inoue, H. Yano and E. Tahara, *J. Gen. Fam. Med.*, 2020, **21**, 143–145.
10 K. Satoh, F. Nagai, T. Seto and H. Yamauchi, *Yakugaku Zasshi*, 2001, **121**, 173–178.
11 L. Xiao and Y. Li, *Zhongguo Zhong Xi Yi Jie He Za Zhi*, 2013, **33**, 298–302.
12 Y. Hirano, H. Isai, A. Onuki and K. Watanabe, *Surg. Neurol. Int.*, 2020, **11**, 80.
13 C. Xu, R. Yue, X. Lv, T. Wu, M. Yang and Y. Chen, *Medicine*, 2020, **99**, e19922.
14 K. K. Jia, Y. J. Zheng, Y. X. Zhang, J. H. Liu, R. Q. Jiao, Y. Pan and L. D. Kong, *J. Ethnopharmacol*, 2017, **209**, 219–229.
15 L. Wang, W. G. Wu, G. X. Li, H. Y. Chen, Y. Y. Fan, W. Chen, G. F. Zhou and W. L. Li, *Phytochem. Anal.*, 2024, 14, DOI: **10.1002/pca.3471**.

16 L. Chen, Y. Cao, H. Zhang, D. Lv, Y. Zhao, Y. Liu, G. Ye and Y. Chai, *J. Ethnopharmacol.*, 2018, **219**, 359–368.
17 Y. Li, W. Yang, W. Li and T. Wu, *J. Pharm. Biomed. Anal.*, 2023, **234**, 115540.
18 R. Li, Y. Zhu, M. Ma, M. Lei, Y. Zhao, T. Liu, M. Yu, Y. Zhao and Z. Yu, *J. Sep. Sci.*, 2022, **45**, 1020–1030.
19 D. Van Der Spoel, E. Lindahl, B. Hess, G. Groenhof, A. E. Mark and H. J. Berendsen, *J. Comput. Chem.*, 2005, **26**, 1701–1718.
20 H. Lutz, V. Jaeger, T. Weidner and B. L. de Groot, *J. Chem. Theory Comput.*, 2019, **15**, 698–707.
21 L. Kagami, A. Wilter, A. Diaz and W. Vranken, *Bioinformatics*, 2023, **39**, btad350.
22 Q. Chen, Q. Zhan, Y. Li, S. Sun, L. Zhao, H. Zhang and G. Zhang, *J. Evidence-Based Complementary Altern. Med.*, 2017, **2017**, 5140297.
23 B. Li, Q. Xiao, J. Zhang, Y. Wang, J. Liu, B. Zhang and H. Liu, *J. Ethnopharmacol.*, 2023, **301**, 115769.
24 M. M. Gravandi, S. Fakhri, S. N. Zarneshan, A. Yarmohammadi and H. Khan, *Metab. Brain Dis.*, 2021, **36**, 1501–1521.
25 D. M. Eskander, W. M. Aziz, M. I. Nassar and M. A. Hamed, *Biomarkers*, 2021, **26**, 606–616.
26 K. M. Wen, X. C. Fang, J. L. Yang, Y. F. Yao, K. S. Nandakumar, M. L. Salem and K. Cheng, *Curr. Med. Chem.*, 2021, **28**, 1042–1066.
27 G. Zhang, S. Chen, W. Zhou, J. Meng, K. Deng, H. Zhou, N. Hu and Y. Suo, *Food Chem.*, 2018, **269**, 150–156.
28 X. L. Jiang, Y. Zhu, G. F. Ma, P. Liu and L. L. Chen, *J. Pharm. Biomed. Anal.*, 2023, **227**, 115276.
29 D. Zhitnitsky, J. Rose and O. Lewinson, *Sci. Rep.*, 2017, **7**, 44554.
30 X. Gao, Y. Ma, Z. Wang, R. Bia, P. Zhang and F. Hu, *Biomed. Chromatogr.*, 2018, **32**, e4179.
31 L. L. Hong, Y. Zhao, C. Y. Yang, G. Z. Li, H. S. Wang, W. D. Chen, X. Y. Cheng and L. Liu, *J. Sep. Sci.*, 2021, **44**, 4327–4342.
32 P. Wang, W. S. Meng, Y. Huang, T. Liu, Y. T. Li, M. Y. Chi, Z. P. Gong and L. Zheng, *Zhongguo Zhong Yao Za Zhi*, 2022, **47**, 6333–6339.
33 K. K. Tatapudi, S. Bandi, N. K. Nagendla, D. R. Solipeta, M. K. R. Mudiam and S. B. Katragadda, *J. Pharm. Biomed. Anal.*, 2023, **235**, 115675.
34 X. Li, P. Lu, W. Zhang, B. Li, R. Yang and K. Luo, *Afr. J. Tradit., Complementary Altern. Med.*, 2013, **10**, 380–385.
35 Y. Shen, P. Zhai, P. Xi, C. Chen, F. Mou, F. Li and J. Zhang, *Rapid Commun. Mass Spectrom.*, 2019, **33**, 1739–1750.
36 L. Li, Z. T. Zuo and Y. Z. Wang, *Am. J. Chin. Med.*, 2022, **50**, 389–440.
37 Y. Zhang, Y. Cheng, Z. Liu, L. Ding, T. Qiu, L. Chai, F. Qiu, Z. Wang, W. Xiao, L. Zhao and X. Chen, *J. Chromatogr. B:Anal. Technol. Biomed. Life Sci.*, 2017, **1061–1062**, 474–486.
38 J. O. Unuofin, N. P. Masuku, O. K. Paimo and S. L. Lebelo, *Front. Pharmacol.*, 2021, **12**, 779352.
39 H. C. Lan, S. Z. Li, K. Li and E. H. Liu, *J. Sep. Sci.*, 2021, **44**, 2046–2053.
40 J. Wang, B. Ouyang, R. Cao and Y. Xu, *Biomed. Chromatogr.*, 2024, **38**, e5784.
41 B. Ma, T. Lou, T. Wang, R. Li, J. Liu, S. Yu, H. Pei, S. Tian, Y. Li, Y. Guo, Z. Wang, Z. Lin, Z. Wang, J. Wang and Y. Gao, *Arabian J. Chem.*, 2021, **14**, 102954.
42 Y. He, W. W. Su, T. B. Chen, X. Zeng, Z. H. Yan, J. M. Guo, W. Yang and H. Wu, *J. Pharm. Biomed. Anal.*, 2019, **176**, 13.
43 J. Chen, X. L. Cheng, L. F. Li, S. Y. Dai, Y. D. Wang, M. H. Li, X. H. Guo, F. Wei and S. C. Ma, *J. Pharm. Biomed. Anal.*, 2022, **207**, 9.
44 X. Y. Zhang, K. R. Xia, Y. N. Wang, P. Liu, E. X. Shang, C. Y. Liu, Y. P. Liu, D. Qu, W. W. Li, J. A. Duan, Y. Chen and H. Q. Zhang, *J. Ethnopharmacol.*, 2024, **325**, 117869.
45 K. Nurmi, K. Silventoinen, S. Keskitalo, K. Rajamäki, V. P. Kouri, M. Kinnunen, S. Jalil, R. Maldonado, K. Wartiovaara, E. I. Nievas, S. P. Denita-Juárez, C. J. A. Duncan, O. Kuismin, J. Saarela, I. Romo, T. Martelius, J. Parantainen, A. Beklen, M. Bilicka, S. Matikainen, D. C. Nordström, M. Kaustio, U. Wartiovaara-Kautto, O. Kilpivaara, C. Klein, F. Hauck, T. Jahkola, T. Hautala, M. Varjosalo, G. Barreto, M. R. J. Seppänen and K. K. Eklund, *Cell Rep. Med.*, 2024, **5**, 101503.
46 Y. Mendoza-Marí, A. García-Ojalvo, M. Fernández-Mayola, N. Rodríguez-Rodríguez, I. Martinez-Jimenez and J. Berlanga-Acosta, *Scars Burn Heal*, 2022, **8**, 20595131211067380.
47 M. Jankovic, N. Spasojevic, H. Ferizovic, B. Stefanovic, K. Virijevic, M. Vezmar and S. Dronjak, *Mol. Neurobiol.*, 2024, **61**, 1495–1506.
48 X. Zhang, Y. Wang and J. Lv, *Neurochem. Int.*, 2024, **175**, 105683.
49 A. Oprita, S. C. Baloi, G. A. Staicu, O. Alexandru, D. E. Tache, S. Danoiu, E. S. Micu and A. S. Sevastre, *Int. J. Mol. Sci.*, 2021, **22**, 587.
50 C. Lu, Y. Song, J. Zhang, Y. Du, T. Wang, Y. Xue, F. Fu and L. Zhang, *Exp. Ther. Med.*, 2014, **7**, 990–994.
51 C. Li and M. H. Wang, *Korean J. Plant Resources*, 2014, **27**, 223–228.
52 S. Guo, K. Jiang, H. Wu, C. Yang, Y. Yang, J. Yang, G. Zhao and G. Deng, *Front. Pharmacol.*, 2018, **9**, 982.
53 C. H. Huang, P. L. Kuo, Y. L. Hsu, T. T. Chang, H. I. Tseng, Y. T. Chu, C. H. Kuo, H. N. Chen and C. H. Hung, *J. Med. Food*, 2010, **13**, 391–398.
54 P. A. Lapchak and P. D. Boitano, *J. Neurol. Neurophysiol.*, 2014, **5**, 214.
55 R. H. Patil, R. L. Babu, M. Naveen Kumar, K. M. Kiran Kumar, S. M. Hegde, G. T. Ramesh and S. Chidananda Sharma, *Mol. Cell. Biochem.*, 2015, **403**, 95–106.
56 Z. Javed, H. Sadia, M. J. Iqbal, S. Shamas, K. Malik, R. Ahmed, S. Raza, M. Butnariu, N. Cruz-Martins and J. Sharifi-Rad, *Cancer Cell Int.*, 2021, **21**, 189.
57 M. Song, L. Li, M. Li, Y. Cha, X. Deng and J. Wang, *Fitoterapia*, 2016, **115**, 31–36.
58 J. Liu, C. Zhang, Z. Liu, J. Zhang, Z. Xiang and T. Sun, *Spine*, 2015, **40**, 363–368.
59 L. K. Chao, P. C. Liao, C. L. Ho, E. I. Wang, C. C. Chuang, H. W. Chiu, L. B. Hung and K. F. Hua, *J. Agric. Food Chem.*, 2010, **58**, 3472–3478.

60 P. S. Yeh, W. Wang, Y. A. Chang, C. J. Lin, J. J. Wang and R. M. Chen, *Cancer Lett.*, 2016, **370**, 66–77.
61 X. Cai, X. Jiang, M. Zhao, K. Su, M. Tang, F. Hong, N. Ye, R. Zhang, N. Li, L. Wang, L. Xue, Z. Zhu, L. Chen, J. Yang, W. Wu and H. Ye, *Phytomedicine*, 2023, **109**, 154617.
62 W. L. Li, X. C. Zhao, Z. W. Zhao, Y. J. Huang, X. Z. Zhu, R. Z. Meng, C. Shi, L. Yu and N. Guo, *J. Asian Nat. Prod. Res.*, 2016, **18**, 1178–1185.
63 C. Cheng and X. Yu, *Int. J. Mol. Sci.*, 2021, **22**, 11078.
64 B. Xue, Y. Zhao, Q. Miao, P. Miao and Y. Zhang, *Biomed. Chromatogr. Bmc*, 2015, **29**, 1235–1248.
65 J. Zhou, J. B. Sun, P. Zheng, J. Liu, Z. H. Cheng, P. Zeng and F. Q. Wang, *Anal. Bioanal. Chem.*, 2012, **403**, 1951–1960.
66 X. Tian, Z. Li, Y. Lin, M. Chen, G. Pan and C. Huang, *Anal. Bioanal. Chem.*, 2014, **406**, 841–849.
67 D. Tang, K. Chen, L. Huang and J. Li, *Expert Opin. Drug Metab. Toxicol.*, 2017, **13**, 1–8.
68 M. Böhmdorfer, A. Maier-Salamon, B. Taferner, G. Reznicek, T. Thalhammer, S. Hering, A. Hüfner, W. Schühly and W. Jger, *J. Pharm. Sci.*, 2011, **100**, 3506–3516.
69 X. Wu, X. Chen and Z. Hu, *Talanta*, 2003, **59**, 115–121.